Multiomics reveals gut dysbiosis contributes to fatty acid dysmetabolism in early phase of acute myocardial infarction

Authors

Yong Fan[a], Jiajun Ying[a,b,c], Ning Huangfu[a,b,c], Kewan He[a,d], Teng Hu[a], Pengpeng Su[e], Xintao Hu[a], Hequn He[f], Wei Liang[g], Junsong Liu[b], Jinsong Cheng[b], Shiqi Wang[b], Ruochi Zhao[b], Hengyi Mao[b], Fuwei He[b], Jia Su[b], Honglin Zhou[b], Zhenwei Li[b], Xiaohong Fei[b], Xiafei Sun[b], Peipei Wang[b], Minfang Guan[b], Weiping Du[b], Shaoyi Lin[b], Yong Wang[b], Fangkun Yang[a], Renyuan Fang[b], Ziqing Kong[h], Xiaomin Chen[a,b,c *], Hanbin Cui[a,b,c *]

Yong Fan and Jiajun Ying contributed equally to this work.

Affiliations

[a] Key Laboratory of Precision Medicine for Atherosclerotic Diseases of Zhejiang Province, The First Affiliated Hospital of Ningbo University, Ningbo 315000, China.

[b] Cardiology Center, The First Affiliated Hospital of Ningbo University, Ningbo 315000, China.

[c] Ningbo Clinical Research Center for Cardiovascular Disease, Ningbo 315000, China.

[d] Present address: Department of Ultrasound, The Affiliated Hospital of Ningbo University, LiHuiLi Hospital, Ningbo 315040, China.

[e] Wenzhou Medical University, Wenzhou 325035, China.

[f] Department of Emergency, The First Affiliated Hospital of Ningbo University, Ningbo 315000, China.

[g] Clinical Laboratory, The First Affiliated Hospital of Ningbo University, Ningbo 315000, China.

[h] Calibra Lab in DI'AN Diagnostics, Key Laboratory of Digital Technology in Medical Diagnostics of Zhejiang Province, Hangzhou 310030, China.

* Corresponding author: X.C. (email: chxmin@hotmail.com) or
H.C. (email: hbcui_nbdyyy@outlook.com)

Abstract

Background: Acute myocardial infarction (AMI) remains a major cause of death, with limited understanding of its early risk stratification. While late-stage AMI has recognized associations with gut microbiome disturbances, the connection to eAMI is less explored.

Methods: Using metabolomics and metagenomics, we analyzed 56 samples, comprising 30 eAMI patients (within 12 hours of onset) and 26 age- and gender-matched healthy controls, to discern the influence of gut microbes and their metabolites.

Results: We found the eAMI plasma is dominated by increased long-chain fatty acids (LCFAs), 14 of which provide differentiating power of eAMI patients from HCs. Multiomics analysis reveals up to 70% of the variance in LCFAs of eAMI patients can be explained by altered gut microbiome. Higher-resolution profiling of gut bacterial species demonstrated that bacterial structural variations are mechanistically linked to LCFAs dysregulation. By *in silico* molecular docking and *in vitro* thrombogenic assay in isolated human platelets, we highlighted that eAMI-associated LCFAs contribute to platelet aggregation, a driving factor for AMI initiation.

Conclusions: LCFAs hold significant potential as early biomarkers of AMI and gut microbiome contributes to altered LCFAs in eAMI. Further studies are imperative to expand upon these observations to better leverage LCFAs as a potential biomarker for eAMI and as a therapeutic target for inhibition of platelet aggregation in eAMI.

53 ## Introduction

54 Acute myocardial infarction (AMI), the most lethal type in coronary artery disease
55 (CAD) and primary cause leading to human mortality and morbidity(1-3), is mainly
56 resulted from the rupture or erosion of atherosclerotic plaque, accompanied by the
57 formation of an occlusive or sub-occlusive thrombus in one or more coronary artery
58 branches(4,5). Accordingly, AMI is divided into two subtypes, ST-segment elevation
59 myocardial infarction (STEMI) and non-ST-segment elevation myocardial infarction
60 (NSTEMI). It has been showed that systemic or local inflammation, imbalance in
61 adaptive immune pathways can modulate atherosclerotic plaque activity and
62 contribute to coronary dysfunction and myocardial ischemic necrosis(5-7). However,
63 the exact underlying mechanism responsible for the progression of coronary artery
64 disease and occurrence of adverse event remains unclear.

65 A rising body of epidemiological study suggests that gut microbiota have a pivotal
66 role in low-grade inflammatory metabolic diseases such as obesity(8) and
67 diabetes(9), which are considered risk factor for atherosclerotic development.
68 Thereafter, pathological evidence indicates that bacteria from the gut or the oral
69 cavity might translocate to and reside in atherosclerotic plaques and could affect the
70 development of atherosclerotic cardiovascular disease (ASCVD)(10,11). Improved
71 sequencing technology and bioinformatics analyses have provided the several
72 significant associations between the microbiota taxa and ASCVD(12,13).

73 On how gut microbiota promote to the development of ASCVD, we have summarized
74 recent advances in the atherosclerosis-linked alterations in gut microbiome,
75 highlighting the microbiota-related circulating metabolites that accelerate the
76 development of ASCVD(14). Microbiota-synthesized metabolites such as
77 trimethylamine N-oxide, secondary bile acids, short-chain fatty acids,
78 lipopolysaccharides and phenylacetylglutamine have been recognized as the
79 important contributor to atherosclerotic consequences. Nevertheless, whether gut
80 microbiota participate in the initiation of AMI, some observational study reported
81 the statistical correlation between gut bacteria profiling and AMI clinical phenotype.
82 However, results are inconsistent across previous findings(15,16).

So far, the reported investigations on the associations between intestinal microbes and AMI recruited mostly patients in the late or stable stage of AMI, sparse report on very early phase of disease has been shown. Whether gut microbes contribute to the early stage of AMI (eAMI) lesion through its derived metabolites remains unknown. Here, we recruited a cohort of 30 patients with eAMI within 12 hours and 26 normal controls, for whom we performed metagenomic sequencing of the gut microbiome and plasma metabolomics. We found that long-chain fatty acids (LCFAs) dominate the metabolome perturbations in eAMI plasma, and the gut microbiome at species level explains up to 70% of the variance in LCFAs composition in eAMI patients. We also found that eAMI-associated LCFAs may possess potent thrombogenic functionality by molecular docking and platelet aggregation assay, which furtherly supports the rational for causal relationship between altered gut microbiota and the initiation of AMI.

98 ## Materials and methods

99 ### Study design and cohort description

100 This study enrolled 30 AMI patients and 26 normal controls who were hospitalized in
101 the First Affiliated Hospital of Ningbo University from February 2021 to November
102 2021. Participants were in strictly conformity with the inclusion and exclusion criteria
103 (**Figure S1**). The diagnosis of AMI is based on the guidelines of the American Heart
104 Association (ACC) in 2021(17).

105 Inclusion criteria were diagnoses of AMI defined as follows: cardiac troponin (cTn)
106 I/T > the upper limit of the 99% normal reference value and have any one or more of
107 the following: significant chest pain of myocardial ischemia; changes in newly
108 diagnosed ischemic electrocardiogram (ST-T changes or left bundle branch block or
109 pathological Q wave); imaging evidence suggested new loss of myocardial activity or
110 regional wall motion abnormalities; abnormal coronary angiography.

111 Exclusion criteria were: history of digestive diseases; severe hepatic and renal
112 dysfunction; history of autoimmune diseases, malignant hematological diseases and
113 tumor; infection within one month of the study or the use of antibiotic or probiotic.
114 Normal controls were hospitalized for health examination at the same period.

115 The study protocol was approved by the Ethics Committee of The First Affiliated
116 Hospital of Ningbo University (No. 2021-R018-YJ01). The study was performed in
117 accordance with the principles of the Declaration of Helsinki. All participants
118 provided written, informed consent for participation in the study.

119 ### Sample collection and biochemical analysis

120 Peripheral venous blood was drawn immediately after the patients arrived at the
121 emergency department, or first moments after hospitalization for normal control
122 individuals. Blood samples were centrifuged immediately at 4 °C, 4000 rpm for 10
123 minutes, and the supernatant (plasma) was stored at −80 °C for further analysis. The
124 first morning fresh fecal (each 400-600 mg) and urine samples were collected from all

125 the participants under the hospital diet, then placed into sterile cryotube and frozen
126 at -80°C refrigerator before further use.

127 Whole blood samples for biochemical measurements were collected after at least 10-
128 hour fasting period. The measurements of fasting glucose, lactate dehydrogenase,
129 creatine kinase, c-reactive protein, serum alanine aminotransferase, aspartate
130 aminotransferase, glutathione S-transferase, creatinine, glycated serum protein, high-
131 density lipoprotein cholesterol, low-density lipoprotein cholesterol, apolipoproteins,
132 lipoprotein, and serum amyloid A were performed by an autoanalyzer (AU5800,
133 Beckmancoulter). HbA1C was measured by an automated clinical analyzer (H100plus,
134 Lifotronic). Plasma brain natriuretic peptide level was measured by a full-automatic
135 chemiluminescence immunoassay analyzer (Cobas e602, Roche). Plasma troponin
136 was measured using an autoanalyzer (DXI800, Beckmancoulter). Urine samples were
137 analyzed by urine sediment analyzer (UF-5000, Sysmex).

138 **Pseudo-targeted metabolomics profiling and preprocessing**

139 Metabolomic profiling was performed utilizing the CalOmics metabolomics platform
140 at Calibra Lab, affiliated with DIAN Diagnostics. The analytical instrumentation
141 comprised an ACQUITY 2D UPLC system (Waters, Milford, MA, USA) coupled with a Q
142 Exactive (QE) hybrid Quadrupole-Orbitrap mass spectrometer (Thermo Fisher
143 Scientific, San Jose, USA). Metabolites were analyzed, based on the chemical
144 properties of the serum metabolites, utilizing both polar ionic and lipid modes.

145 Sample preparation involved the extraction of metabolites using a methanol solvent
146 at a 1:4 ratio. Following extraction, mixtures were shaked for three minutes and
147 subsequently subjected to centrifugation at 4000 × g for 10 minutes at 20°C to
148 precipitate proteins. The resulting 100 µL aliquots of supernatant were transferred
149 onto sample plates, dried under a stream of nitrogen, and reconstituted in
150 appropriate solvents for injection into the UPLC-MS/MS system.

151 The QE mass spectrometer settings included a mass resolution of 35,000 and a scan
152 range from 70 to 1000 m/z. For the first UPLC-MS/MS method, the instrument

153 operated in positive electrospray ionization (ESI) mode using a C18 reverse-phase
154 UPLC column (UPLC BEH C18, 2.1x100 mm, 1.7 µm; Waters). The mobile phases
155 consisted of water (A) and methanol (B) with 6.5 mM ammonium bicarbonate at pH
156 8 for gradient elution. The third method similarly employed the C18 reverse-phase
157 column in ESI positive mode, but used a mobile phase of water (A) and a mixture of
158 methanol, acetonitrile, and water (B) containing 0.05% perfluoropentanoic acid
159 (PFPA) and 0.01% formic acid (FA). In the fourth method, the system was operated in
160 negative ESI mode with a hydrophilic interaction liquid chromatography (HILIC)
161 column (UPLC BEH Amide, 2.1x150 mm, 1.7 µm; Waters), and the mobile phases
162 were water (A) and acetonitrile (B) containing 10 mM ammonium formate.

163 Following the preprocessing of raw data and rigorous data quality control
164 assessments, ion peaks were extracted employing proprietary in-house information
165 technology hardware and software systems. Metabolites were subsequently
166 identified through querying a bespoke library, which was compiled using pure
167 standards sourced from commercial providers or other available channels. The
168 identification protocol for metabolites within the samples was stringent, requiring a
169 precise match across three specific criteria when compared to the library entries: a
170 narrow retention index window, mass accuracy within a 10 ppm deviation, and
171 tandem mass spectrometry (MS/MS) spectra that exhibit high scores in both forward
172 and reverse searches. Quantification of each metabolite was achieved by calculating
173 the peak area using the area-under-the-curve (AUC) method. This approach ensures
174 accurate measurement of metabolite concentrations within the samples.

175 Before statistical analysis, raw peak areas were normalized to adjust for system
176 fluctuation among different run days. The normalized peak areas were then log-
177 transformed (log2) to reduce data distribution skewness and be in approximate
178 normal distribution (Gaussian distribution). Missing values in peak area matrix were
179 imputed by using the minimal detection value of a metabolite among all tested
180 samples.

181 **DNA extraction and library construction of fecal samples**

182 Deoxyribonucleic acid (DNA) was extracted from fecal samples utilizing the
183 cetyltrimethylammonium bromide (CTAB) method. Control samples included unused
184 swabs which were processed identically through the DNA extraction protocol to
185 ensure absence of DNA amplification products. The resultant DNA was eluted in 50 µl
186 of elution buffer, following a modified protocol provided by QIAGEN, and preserved
187 at -80°C for subsequent analyses.

188 For polymerase chain reaction (PCR) analysis, the samples were processed at LC-BIO
189 Technologies Co., Hangzhou, China. The construction of the DNA library was
190 accomplished using the TruSeq Nano DNA LT Library Preparation Kit (FC-121-4001).
191 Fragmentation of the DNA was performed using dsDNA Fragmentase (NEB, M0348S)
192 at 37°C for 30 minutes. This step produced blunt-ended DNA fragments via a
193 combination of fill-in reactions and exonuclease activity. Size selection was then
194 conducted using the sample purification beads provided in the kit.

195 To prepare the DNA fragments for adapter ligation, an adenine (A) base was added to
196 the blunt ends of each strand. Each adapter, designed with a thymine (T) base
197 overhang, facilitates the ligation to the A-tailed DNA fragments. These adapters are
198 crucial as they contain necessary sites for the hybridization of sequencing primers,
199 enabling single, paired-end, and indexed sequencing reads.

200 Ligation involved either single or dual index adapters, and the products were
201 subsequently amplified via PCR. The amplification parameters included an initial
202 denaturation at 95°C for 3 minutes, followed by 8 cycles of denaturation at 98°C for
203 15 seconds, annealing at 60°C for 15 seconds, extension at 72°C for 30 seconds, and a
204 final extension at 72°C for 5 minutes. This process prepares the library for high-
205 throughput sequencing analyses.

206 **Metagenomic sequencing data processing**

207 Raw sequencing data were processed to generate clean reads suitable for
208 downstream analyses. Initially, sequencing adapters were excised from the reads
209 using Cutadapt (version 1.9). Subsequently, low-quality reads were trimmed using
210 fqtrim (version 0.94), which employs a sliding-window algorithm. Reads were then

211 aligned to the host genome using Bowtie2 (version 2.2.0) to eliminate host-derived
212 sequences. Following the quality filtering, the remaining reads were assembled de
213 novo using IDBA-UD (version 1.1.1) to construct individual metagenomes for each
214 sample. Predictions of coding regions (CDS) within the metagenomic contigs were
215 performed by MetaGeneMark (version 3.26). The CDS sequences across all samples
216 were clustered using CD-HIT (version 4.6.1) to generate a set of unigenes. Unigene
217 abundance in each sample was estimated using transcripts per million (TPM) based
218 on read alignment performed again with Bowtie2 (version 2.2.0). Taxonomic
219 classification of the unigenes was achieved by aligning them to the NCBI non-
220 redundant (NR) database using DIAMOND (version 0.9.14). The taxonomic
221 annotations and abundance profiles of these unigenes were utilized to conduct
222 differential analysis at both taxonomic and gene-specific levels. Enterotypes profiling
223 was performed using pipeline as previously demonstrated (18). Phage-inclusive
224 metagenomics profiling was conducted with Phanta.

225 **Profiling of bacterial structural variations**

226 Prior to the structural variations (SVs) classification, the iterative coverage-based
227 read assignment pipeline was used to precisely reassign the ambiguous reads to the
228 most likely reference(19,20). The reference genomes given in the proGenomes
229 database (http://progenomes1.embl.de/) were concatenated, separated into
230 genomic 1-kbp bins, and used for the detection of highly variable genomic variations.
231 The SGV-Finder pipeline(19) was used to identify SVs that fall into one of three
232 categories: (1) variable SVs, or vSVs, (2) deletion SVs, or dSVs; the presence or
233 absence of a specific genomic segment was maintained; or (3) deletion SVs, or dSVs,
234 with deletion percentages of >75% (this genomic segment was excluded from the
235 analysis). All bacterial species with SV calling were found in at least 10% of all
236 samples and were used in the analysis that followed.

237 **Molecular docking simulation**

238 The crystal structures of several human receptors were obtained from the RCSB
239 Protein Data Bank (https://www.rcsb.org/). These include the free fatty acid receptor

240 1 (GPR40, PDB ID: 5TZY), the thromboxane A2 receptor (TXA2, PDB ID: 6IIV), and the
241 P2Y purinoceptors 1 and 12 (PDB IDs: 4XNW and 7PP1, respectively). Subsequent to
242 download, water molecules and co-crystallized ligands were removed from the .pdb
243 files to prepare the proteins for molecular docking studies. For the docking
244 simulations, the receptor structures were prepared by adding polar hydrogen atoms
245 and computing partial charges using the Kollman and Gasteiger methods. These
246 modifications were performed using AutoDock Tools (version 1.5.638). The prepared
247 structures of both ligands and receptors were then saved in .pdbqt format,
248 facilitating their use in subsequent molecular docking procedures. The molecular
249 docking studies were performed using the open-source software AutoDock Vina
250 (version 1.1.2) (21) investigate the interactions between AMI-associated long-chain
251 fatty acids (LCFAs) and selected receptors involved in platelet aggregation.
252 Adjustments to the grid box allowed the AutoDock algorithm to predict ligand
253 conformations within the receptor binding sites and evaluate them using scoring
254 functions (22), with the grid spacing set at 1 Å. The three-dimensional interactions
255 between the selected receptors and long-chain fatty acids (LCFAs) were analyzed and
256 visualized using the PyMOL Molecular Graphics System (version 2.5.0), an open-
257 source platform. Subsequently, AutoDock version 4.2 was employed to predict the
258 binding affinities between various ligands and the selected receptors, providing
259 quantitative insights into the potential binding interactions (23).

260 **Thrombogenic effect of LCFAs on isolated human platelets**

261 Fresh platelets were obtained from normal human volunteers without any
262 antiplatelet or anticoagulant drugs being used within 2 weeks. Whole blood was
263 collected from the peripheral vein of healthy volunteers into 0.1 vol of ACD buffer (75
264 mM sodium citrate, 39 mM citric acid, and 135 mM dextrose, pH 6.5). Diluted whole
265 blood was centrifuged at 1500g for 20 minutes at 25 ^{o}C, and platelet-rich plasma
266 (PRP) was collected into a fresh tube. Then we diluted PRP in ACD buffer, and
267 centrifuged it at 800g for 10 minutes at 25℃. The platelet pellet was then
268 resuspended in Tyrode's buffer (137 mM NaCl, 2 mM KCl, 0.34 mM Na_2HPO_4, 12 mM

269 $NaHCO_3$, 1 mM $MgCl_2$, 5.5 mM glucose, 5 mM HEPES, and 0.35% BSA, pH 6.5) at 10^9
270 platelets/mL, and kept at 23 °C for up to 4 h before use.

271 Incubations of washed human platelets with fatty acids were done either in pH 6.5
272 phosphate buffer or in "pH 7.4 Tris buffer" (15.4 mM Tris-Cl, pH 7.4; 140 mM NaCl,
273 5.6 mM glucose(24)). Candidate LCFAs to be tested were chosen according to the
274 results shown in **Figure 2a**. Then individual LCFA was diluted to specific concentration
275 (1 mM, 2.5mM, 5mM and 10mM) by bovine serum albumin solution (BSA),
276 respectively. Platelet aggregations were measured using a lumi-aggregometer
277 (AG800, Shandong, China) at 37 ^{o}C under stirring at 1200 rpm.

278 **Statistical analysis**

279 In this study, no data were excluded before the statistical analysis. As the study is
280 observational, no allocation or randomization was used. This study includes all
281 available samples (n = 56) of patients with AMI and healthy individuals. Although
282 sample sizes were not predetermined using statistical methods, our sample sizes are
283 comparable to those published earlier(25,26). The distribution of samples among
284 metagenomics and metabolomics batches was random. During the data collecting
285 phases of the metagenomic, biochemical, and metabolomics, researchers were
286 blinded to the group allocation.

287 All statistical analyses were performed with R (version 4.2.3). Significantly differed
288 metabolites or taxa between AMI and control groups were found by parametric
289 (student's *t*-test) or non-parametric (Wilcox's rank test) statistical methods.
290 Multivariate analysis approaches including principal component analysis (PCA),
291 principal coordinate analysis (PCoA), and random forest (RF) were also conducted.
292 Permutational multivariate ANOVA (PERMANOVA) was performed to determine the
293 differences in structures of global microbiome and LCFAs between AMI patients and
294 controls by using *vegan* (v2.6-4) package. The association analysis between omics
295 features were performed by spearman correlation using *cor.test* base command.
296 Least absolute shrinkage and selection operator (LASSO) regression model was built
297 by using *glmnet* (v4.1-7) package. Unless otherwise stated, all p values were

298 corrected using the Benjamini-Hochberg method andz Padj < 0.05 was considered
299 statistically significant.

300

301 ## Results

302 **Plasma metabolome and gut microbiome from a deeply phenotyped eAMI cohort**

303 We profiled plasma samples collected from 30 early acute myocardial infarction
304 (eAMI) patients (within 12 hours in emergency) and 26 age- and gender-matched
305 healthy controls (HC), using mass spectrometry. For these participants, we also
306 characterized gut microbiota by performing shotgun metagenomic sequencing of
307 fecal samples. In addition, as shown in **Table 1**, it is important to note that HC in this
308 study had no obstructions in in any of their coronary arteries, which was validated by
309 coronary angiography, in addition to having bioclinical characteristics that were
310 within heathy thresholds. As expected, eAMI patients are distinct from HC with
311 elevated troponin, pro-BNP, and creatine kinase (p values < 1.0e-03) despite
312 matching for age, sex, BMI and T2D status. Also, eAMI patients display increased
313 inflammatory markers including C-reactive protein, white blood cells, neutrophils,
314 and lymphocytes (p values < 1.0e-03).

315 A pseudo-targeted metabolomics platform was used to profile 926 identified
316 metabolites, as well as 26 partially characterized features (**Table S1**). Metabolites
317 belonged to diverse biochemical classes, including lipids, amino acids, xenobiotics,
318 nucleotides, and carbohydrates (**Figure S2a**). Most metabolites (877) were measured
319 in over 50% of the cohort, and 555 metabolites were present in all samples (**Figure**
320 **S2b**). All the samples were randomly injected and median of RSDs for the internal
321 standards used in the quality control samples is 2.78%, demonstrating the high
322 quality of metabolomics data.

323 Bacterial DNA was extracted from fecal samples, sequenced on the Illumina platform,
324 and a total of 402 Gb 150-bp paired-end reads were generated, with an average of
325 47.70 ± 5.98 (s.d.) million reads per sample (**Table S2**). For each sample, a majority of

326 high-quality sequencing reads (69.03–97.24%) were *de novo* assembled into long
327 contigs or scaffolds, which were used for gene prediction, taxonomic classification,
328 and profiling of structural variations (SVs) in bacterial genomes.

329 **LCFAs dominate the metabolome perturbations in eAMI plasma**

330 Principal component analysis of the 952 measured compounds is used in **Figure 1a** to
331 show the remarkable differences in the global plasma metabolome of eAMI patients
332 compared to HC subjects and individual contrasted metabolites are shown in **Figure**
333 **S3**. To characterize the dysregulated metabolic pathways in patients with eAMI, we
334 performed KEGG pathway enrichment analysis of the differential metabolites and
335 observed that biosynthesis of unsaturated fatty acids (FA) was the most significantly
336 disrupted in eAMI patients (**Figure 1b**). Moreover, we found that across the eAMI and
337 HC groups, the 32 LCFAs species (saturated, monounsaturated, and polyunsaturated)
338 showed considerable inter-individual heterogeneity (**Figure 1c**). Plasma LCFAs
339 composition also displayed a significant variation between the two groups
340 (permutational multivariate analysis of variance (PERMANOVA), $p < 1.0e-03$; **Figure**
341 **1d**), with 28 upregulated LCFAs between patients with eAMI and HC as demonstrated
342 in the volcano plot (**Figure 1e**).

343 Thereafter, we divided our cohort into a training group (comprising 70% of the
344 subjects) and a test set (comprising 30% of the subjects) to identify diagnostic
345 biomarkers for differentiating HC and patients with eAMI. The training dataset was
346 utilized to perform feature selection using LCFAs in plasma, and the selected features
347 were then used to create a random forests classifier (**Figure 2a**). With an area under
348 the receiver operating characteristic curve (AUC) of 0.927 in the training set, the
349 random forests model by a biomarker panel of 14 LCFAs (**Figure 2b**) allowed
350 differentiation between HC and eAMI groups (**Figure 2c**). The created classifier was
351 subsequently used in testing dataset to estimate independent performance of our
352 model, which had an AUC of 1 (**Figure 2d**). Overall, these findings reveal the
353 differences of LCFAs alteration is dominant in metabolome perturbations of patients
354 with eAMI and demonstrate LCFAs may allow to discover more potent biomarkers,
355 making the diagnosis of eAMI more accessible.

356 **Alterations in gut microbiome is associated with the LCFA dysmetabolism in eAMI**

357 We next explored the underlying factors that regulate LCFA metabolism by factor
358 analysis, where we found age, sex, and body mass index could only account for up to
359 10% of the variance in LCFA proportion (**Figure 3a**). This indicates that a large
360 proportion of LCFA variation remains unexplained and may be attributed to other
361 variables, for example, gut microbial factors. Consistent to previous reports(12), we
362 identified that eAMI gut microbiome is not only distinct from but also more
363 heterogenous than that of HC subjects (**Figure S4**). Furthermore, we found eAMI gut
364 microbiome is marked by an enrichment in the Bacterides2 enterotype ($P_{\text{Fisher's exact}}$
365 $_{\text{test}}$ = 2.3e-02) with a slight depletion in Bacteroides1 enterotype ($P_{\text{Fisher's exact test}}$ = 3.1e-
366 01, **Figure 3b**), which always represents a marker suggesting a high risk of metabolic
367 disorders(27).

368 To furtherly understand if gut microbiome is involved in the regulation of LCFAs
369 during the onset of eAMI, we performed a least absolute shrinkage and selection
370 operator (LASSO) regression model to compute the variance in each of the detected
371 LCFAs that can be explained by gut microbiome. Intriguingly, gut microbiome at
372 species level explains up to 70% of the variance in LCFAs composition in this cohort
373 (**Figure 3c**). We next sought to identify the potential bacterial taxa that associate with
374 the LCFAs by spearman correlation. At genus level, *Mycobacteroides*, *Thermus*, and
375 *Anaerostipes* are inversely linked to LCFAs (**Figure S5**). As shown in **Figure 3d**, we
376 found *Streptococcus* species were negatively correlated with omega-3
377 polyunsaturated FAs including FFA 18:4 (n-3), FFA 18:3 (n-3 or -6), and FFA 22:5 (n-3),
378 which were considered as cardioprotective compounds. Meanwhile, the
379 *Streptococcus* species were found to be positively correlated with omega-6
380 polyunsaturated FAs and saturated LCFAs. Moreover, we discovered that the eAMI
381 gut virome exhibits a decrease in *Vibrio* phage (**Figure 4a**) but enrichments in
382 *Streptococcus* phage PH10 and *Streptococcus* phage SM1 (**Figure 4b**), both of which
383 have known hosts that are *Streptococcus* species. *Streptococcus* bacterial species
384 predominate in the eAMI gut microbiome (**Figure S4a**), although the mechanism
385 underpinning this dominance is unclear. Nonetheless, the abundance in temperate
386 lysogenic *Streptococcus* phages may provide some justification. Additionally, the total

387 number of virulent phages found in the eAMI gut microbiome is higher than in the
388 healthy controls (Figure 4c). The ratio of virulent to temperate phages is also greater
389 in the eAMI group compared to the HC group.

390 **Gut bacterial structural variants profiling in eAMI**

391 Structural variations (SVs) in bacterial genomes can disrupt gene function, thereby
392 influencing the interactions between bacteria and their hosts (25). As a result,
393 significant phenotypic and functional alterations within the gut microbiome of
394 patients with early acute myocardial infarction (eAMI) may arise from differences in
395 the presence or levels of SVs among genetically similar bacterial strains. Here, we
396 profiled SVs in all samples and identified 4,234 deletion SVs and 1,948 variable SVs
397 across 47 bacterial species (**Figures 5a** and **5b**). For some species, we observed
398 considerable differences in copy number variation. We identified 87 deletion SVs and
399 18 variable SVs in *Bacteroides uniformis* across 134 individuals, 78 deletions and 15
400 variable SVs in *Faecalibacterium prausnitzii* in 124 individuals, and 110 deletion SVs
401 and 55 variable SVs in *Parabacteroides distasonis* in 121 individuals. For the archaeal
402 microbiota, we only identified SVs in *Methanobrevibacter smithii* in 13 individuals
403 (**Figures 5a**). To explore potential differences in bacterial genetics, we further
404 computed the Canberra distance of bacterial SV profiles between eAMI versus HC
405 (**Figure 5c**). eAMI and HC samples were significantly different in the beta-diversity of
406 SV composition (P_{Wilcoxon} = 1.4e-05) and composition of bacterial genetics in eAMI
407 individuals has less heterogeneity than that of HC subjects.

408 **Bacterial genetics associate to LCFAs dysmetabolism in eAMI**

409 Exploring relationships between gut bacterial SVs and plasma LCFAs, we found that
410 bacterial SVs were significantly related to LCFAs (**Figure 5d**). As a particularly notable
411 example, in the association analysis between SVs in the *Alistipes shahii* genome and
412 plasma LCFAs profile, we found that a 3-kbp deletion (*A. shahii*:575-578) was directly
413 associated with FFA 22:4 and FFA 14:1 but inversely linked to FFA 16:0, indicating that
414 this deletion SV may be involved in the regulation of LCFAs metabolism in eAMI
415 (**Figure 5e**). According to gene analysis, the beginning of this specific genomic region

416 in *A. shahii* encodes a 3-oxoacyl-[acyl-carrier protein] reductase (*FabG*, **Figure 5f**),
417 which is an enzyme catalyzes the NADPH-dependent reduction of beta-ketoacyl-ACP
418 substrates to beta-hydroxyacyl-ACP products, the first reductive step in the
419 elongation cycle of fatty acid biosynthesis. This deletion region is more prevalent in
420 eAMI group compared to HC gut microbiome (**Figure 5g**). In accordance with the
421 association analysis, we furtherly found that individuals with *A. shahii* genomes
422 harboring this deletion have higher plasma FFA 22:4 and FFA 14:1 but lower level of
423 FFA 16:0, compared to participants without this 3-kbp deletion in A. *shahii* genome
424 (**Figure 5h**).

425 **Molecular docking and thrombosis in human platelets support the thrombogenic**
426 **effect of eAMI-associated LCFAs**

427 We extended our work to *in silico* molecular docking to investigate the molecular
428 connections that control thrombosis. Four canonical receptors that are involved in
429 platelet aggregation—free fatty acid receptor 1 (GPR40), thromboxane A2 receptor
430 (TXA2), P2Y purinoceptor 1 (P2Y1), and P2Y purinoceptor 12 (P2Y12)—were taken
431 into account as binding receptors in the molecular docking models in addition to the
432 28 eAMI-associated LCFAs as binding ligands. As shown in **Figure 6a**, we selected the
433 first-ranked complex models between the various LCFAs and these four receptors.
434 Interestingly, the molecular docking models estimated substantial interactions
435 between eAMI-associated LCFAs and four selected receptors, with binding affinity
436 ranging from -5.7 to -9.1 kJ/mol (**Figure 5a**). Representative docking results for
437 bindings between the chosen receptors and omega-3, -6, and -9 polyunsaturated FAs
438 are displayed in **Figure 6b**.

439 Then, using *in vitro* human platelet anticoagulation assay, we aimed to
440 experimentally validate the thrombogenic effects of eAMI-associated LCFAs. As
441 shown in **Figure 6c**, we found omega-6 LCFAs significantly stimulate platelet
442 aggregation at physiological concentrations (1 mM to 10 mM). As a non-ignorable
443 example, FFA 19:1 (n-9), as a non-omega-6 LCFA, also causes strong thrombosis in
444 human platelet (**Figure 6d**), while the mechanistic understanding behind this finding
445 remains unknown. Our results imply suggest that eAMI-associated LCFAs may

446 possess potent thrombogenic functionality, making it fair to assume that they play a
447 significant role in host cardiometabolic health.

448 ## Discussion

449 The factors triggering the onset of AMI and the precise indicators of eAMI remain
450 unclear. However, the application of plasma metabolomics provides valuable insights
451 into the search for accurate diagnostic markers for complex conditions such as AMI.
452 Additionally, comprehensive multi-omics profiling plays a crucial role in unraveling
453 the underlying mechanisms responsible for AMI. Together, these approaches shed
454 light on both diagnostic advancements and a deeper dissection disentangling the
455 complexity of eAMI.

456 By plasma metabolomics profiling, we found that in patients with eAMI, there was a
457 remarkable increase in 28 LCFAs dominating the altered eAMI metabolome. These
458 LCFAs encompassed a variety of saturated, monounsaturated, and polyunsaturated
459 types. When investigating the etiology of LCFA dysmetabolism in eAMI, we initially
460 examined its correlation with conventional AMI risk factors including age, sex, body
461 mass index, and potentially diabetes. However, these factors alone could only explain
462 a maximum of 10% of the variation observed in LCFA proportions. This raises the
463 question of what accounts for the remaining 90% of LCFA variation. To this end, we
464 turned our attention to profiling the gut microbiota, as it is widely recognized for its
465 potential role in regulating the metabolome. The LASSO regression model allows us
466 to examine various factors influencing LCFA composition and reveals gut microbiome
467 at the species level accounted for up to 70% of the observed variance in the
468 composition of LCFAs. This finding suggests a significant association between the gut
469 microbiome and the alterations in LCFA levels.

470 To gain mechanistic insights behind the gut microbiome-LCFA interactions, we
471 associated bacterial SVs with LCFAs and observed significant relations. Of specific
472 interest is a 3-kbp deletion (*A. shahii*: 575-578) representing *FabG* gene, a key
473 enzyme in reduction step of elongation cycle in fatty acid biosynthesis, which is more
474 prevalent in eAMI gut microbiome, resulting in a relatively higher plasma FFA 22:4

475 and FFA 14:1 in eAMI patients. Others have already reported the increase of
476 intracolonic saturated LCFAs positively associated with elevated abundances of
477 *Prevotella, Lactobacillus*, and *Alistipes*(28). Additionally, the presence of *A. shahii* was
478 also shown to strengthen the positive associations of red meat intake with
479 trimethylamine N-oxide (TMAO) concentrations levels(29), while increased TMAO
480 levels enhances platelet hyperreactivity and thrombosis risk(30), and is associated
481 with an increased risk of incident major adverse cardiovascular events(31). These
482 findings support that in addition to short-chain fatty acids – which are known gut
483 microbial products – disturbances in the gut microbiota also contribute significantly
484 to the variation in plasma LCFAs during eAMI.

485 Indeed, the question arises whether the elevated levels of LCFA in eAMI are merely a
486 marker or if they hold pathophysiological significance. Considering that platelet
487 activation is a distinct pathophysiological characteristic of eAMI, we sought to
488 explore the impact of eAMI-associated LCFA on circulating platelet activation. As
489 expected, we found a majority of omega-6 LCFAs rather than omega-3 LCFAs dose-
490 dependently stimulate platelet aggregation. A role for omega-3 polyunsaturated fatty
491 acids (PUFA) supplementation to achieve cardioprotective effects has also been
492 shown by attenuating platelet function(32), aligning with our findings. To date, there
493 is limited conclusive evidence regarding the effect of LCFAs on platelet activation,
494 except for arachidonic acid (FFA 20:4 (n-6)), a well-known LCFA that activates
495 platelets. However, our study has yielded intriguing results. We have discovered that
496 both FFA 19:1 (n-9) (also known as 10-nonadecenoic acid, HMDB0013622) and FFA
497 22:4 (n-6) (Adrenic acid, HMDB0002226) can significantly induce human platelet
498 aggregation to a similar degree as arachidonic acid (FFA 20:4 (n-6), see **Figure S6**).
499 Notably, FFA 22:4 (n-6) can be synthesized from arachidonic acid (FFA 20:4 (n-6)),
500 which, in turn, can be elongated from FFA 18:2 (n-6), also known as linoleic acid.
501 These conversions and interactions among omega-6 PUFAs provide a potential
502 mechanism for their role in activating platelets.

503 Consistent with previous reports(33), the outcome of our *in vitro* experiments
504 supports many eAMI-associated LCFAs, especially omega-6 PUFAs can promote
505 platelet aggregation even in normal physiological concentration (1-5 mM). However,

lots of epidemiological investigation has found higher intakes of omega-6 PUFA appear to be safe and may be even more beneficial, hence the AHA supports an omega-6 PUFA intake of at least 5% to 10% of energy for dietary recommendations of coronary heart disease(34). In another prospective analyses, higher *in vivo* circulating and tissue levels of LA and possibly AA were associated with lower risk of major cardiovascular events(35). Intriguingly, omega-6 PUFA, dihomo-γ-linolenic acid (FFA 20:3 (n-6)) has been shown to play a role in inhibiting platelet aggregation ex vivo, via COX-1–derived prostanoid metabolites(36). Therefore, it still has the overwhelming controversial data on potential effects of omega-6 PUFAs on platelet function.

While our study offered valuable multi-omics insights into a cohort of patients with eAMI, uncovering the association between gut dysbiosis and plasma metabolomic perturbations characterized by the notable enrichment of LCFAs, it is important to acknowledge certain limitations in our present study. Firstly, we propose that intestinal microbial disturbances are significantly associated with fatty acid dysmetabolism based on cross-sectional correlation analysis. However, the causal relationship between gut microbiota dysbiosis and altered FA metabolism remains unclear and requires confirmation in prospective cohorts. Secondly, while platelet activation is a characteristic feature of eAMI, the specific *in vivo* role of LCFAs is still not well understood, and there is ongoing debate regarding the effect of ω-6 LCFAs on platelet function. Thirdly, we still don't know the direct or indirect effect of gut microbiota dysbiosis on platelet activation, as well the underlying mechanism responsible for it, despite there is report on TMAO(30) and phenylacetylglutamine(37) contributing to platelet hyperreactivity and enhanced thrombosis potential. Fourthly, although all participants followed a standardized in-hospital diet and stool samples were collected shortly after hospitalization, the potential influence of pre-hospital diet on intestinal microbiome and plasma metabolome profiling, as well as their interaction, cannot be completely ruled out. Finally, due to the limitations of sample size and the specific population background included in this study, the conclusions drawn from our findings should be furtherly validated through large-scale, prospective studies involving diverse regional populations.

537 ## Data availability

538 The metadata are available under restricted access due to participant consent and
539 privacy regulations of this cohort, access can be obtained by request to the
540 corresponding author. Access to the metagenomics and metabolomics data may be
541 granted for statistical and scientific research with approval from the corresponding
542 author (Hanbin Cui: hbcui_nbdyyy@outlook.com).

543 ## Code availability

544 Scripts associated with the data analysis and visualization are available at
545 https://github.com/fjw536/AMI_gut_microbiome.

546 ## Acknowledgements

547 We thank the study participants and nurses for their contributions to the project. We
548 gratefully acknowledge colleagues at Lianchuan biotechnology for Metagenomics
549 sequencing analysis of gut microbiota, and DI'AN Diagnostics, Key Laboratory of
550 Digital Technology in Medical Diagnostics of Zhejiang Province for plasma
551 metabolomics profilling, data analysis and discussions.

552 ## Author contributions

553 Y.F., J.Y. and H.C. conceived and designed the study. J.Y., F.H., K.H., T.H., H.M., P.S. X.H.,
554 H.M., Z.L., R.Z., J.L., J.C., S.W., X.S., H.H., P.W., M.G., J.S., W.D., Y.W., H.Z., S.L., X.F.,
555 W.L., R.F., F.H. and X.C. were involved in the acquisition of samples and data. Y.F. and
556 Z.K. analyzed and interpreted the data. Y.F. and J.Y. drafted the work and H.C.
557 substantively revised it. All authors contributed to the article and approved the
558 submitted version.

559 ## Competing interests

560 All authors declare no competing interests in this study.

561 ## Funding

This research was supported by the Key research and development project of Zhejiang Province, China (no. 2021C03096), Major Project of Science and Technology Innovation 2025 in Ningbo, China (no. 2021Z134) and Ningbo Clinical Research Center for Cardiovascular Disease, Ningbo, China (no. 2022L001).

567 # Reference

568 1. DALYs GBD, Collaborators H. Global, regional, and national disability-adjusted life years
569 (DALYs) for 306 diseases and injuries and healthy life expectancy (HALE) for 188 countries,
570 1990-2013: quantifying the epidemiological transition. Lancet 2015;386:2145-91.
571 2. Faxen J, Jernberg T, Hollenberg J, Gadler F, Herlitz J, Szummer K. Incidence and Predictors of
572 Out-of-Hospital Cardiac Arrest Within 90 Days After Myocardial Infarction. J Am Coll Cardiol
573 2020;76:2926-2936.
574 3. Gong W, Yan Y, Wang X et al. Risk Factors for In-Hospital Cardiac Arrest in Patients With ST-
575 Segment Elevation Myocardial Infarction. J Am Coll Cardiol 2022;80:1788-1798.
576 4. Anderson JL, Morrow DA. Acute Myocardial Infarction. The New England journal of medicine
577 2017;376:2053-2064.
578 5. Crea F, Libby P. Acute Coronary Syndromes: The Way Forward From Mechanisms to Precision
579 Treatment. Circulation 2017;136:1155-1166.
580 6. Maier W, Altwegg LA, Corti R et al. Inflammatory markers at the site of ruptured plaque in
581 acute myocardial infarction: locally increased interleukin-6 and serum amyloid A but
582 decreased C-reactive protein. Circulation 2005;111:1355-61.
583 7. Granger CB, Kochar A. Understanding and Targeting Inflammation in Acute Myocardial
584 Infarction: An Elusive Goal. J Am Coll Cardiol 2018;72:199-201.
585 8. Turnbaugh PJ, Ley RE, Mahowald MA, Magrini V, Mardis ER, Gordon JI. An obesity-associated
586 gut microbiome with increased capacity for energy harvest. Nature 2006;444:1027-31.
587 9. Karlsson FH, Tremaroli V, Nookaew I et al. Gut metagenome in European women with normal,
588 impaired and diabetic glucose control. Nature 2013;498:99-103.
589 10. Jonsson AL, Backhed F. Role of gut microbiota in atherosclerosis. Nature reviews Cardiology
590 2017;14:79-87.
591 11. Barrington WT, Lusis AJ. Atherosclerosis: Association between the gut microbiome and
592 atherosclerosis. Nature reviews Cardiology 2017;14:699-700.
593 12. Jie Z, Xia H, Zhong SL et al. The gut microbiome in atherosclerotic cardiovascular disease.
594 Nature communications 2017;8:845.
595 13. Karlsson FH, Fak F, Nookaew I et al. Symptomatic atherosclerosis is associated with an altered
596 gut metagenome. Nature communications 2012;3:1245.
597 14. Fan Y, Ying J, Ma H, Cui H. Microbiota-related metabolites fueling the understanding of
598 ischemic heart disease. iMeta 2023;2:e94.
599 15. Kelly TN, Bazzano LA, Ajami NJ et al. Gut Microbiome Associates With Lifetime Cardiovascular
600 Disease Risk Profile Among Bogalusa Heart Study Participants. Circulation research
601 2016;119:956-964.
602 16. Liu M, Wang M, Peng T et al. Gut-microbiome-based predictive model for ST-elevation
603 myocardial infarction in young male patients. Frontiers in microbiology 2022;13:1031878.
604 17. Gulati M, Levy PD, Mukherjee D et al. 2021 AHA/ACC/ASE/CHEST/SAEM/SCCT/SCMR
605 Guideline for the Evaluation and Diagnosis of Chest Pain: A Report of the American College of
606 Cardiology/American Heart Association Joint Committee on Clinical Practice Guidelines. J Am
607 Coll Cardiol 2021;78:e187-e285.
608 18. Vieira-Silva S, Falony G, Belda E et al. Statin therapy is associated with lower prevalence of gut
609 microbiota dysbiosis. Nature 2020;581:310-315.

610 19. Zeevi D, Korem T, Godneva A et al. Structural variation in the gut microbiome associates with
611 host health. Nature 2019;568:43-48.
612 20. Wang D, Doestzada M, Chen L et al. Characterization of gut microbial structural variations as
613 determinants of human bile acid metabolism. Cell Host Microbe 2021;29.
614 21. Trott O, Olson AJ. AutoDock Vina: improving the speed and accuracy of docking with a new
615 scoring function, efficient optimization, and multithreading. J Comput Chem 2010;31:455-
616 461.
617 22. Pahonțu E, Proks M, Shova S et al. Synthesis, characterization, molecular docking studies and
618 in vitro screening of new metal complexes with Schiff base as antimicrobial and
619 antiproliferative agents. Appl Organometal Chem 2019;33:e5185.
620 23. Morris GM, Huey R, Lindstrom W et al. AutoDock4 and AutoDockTools4: Automated docking
621 with selective receptor flexibility. J Comput Chem 2009;30:2785-2791.
622 24. Neufeld EJ, Wilson DB, Sprecher H, Majerus PW. High affinity esterification of eicosanoid
623 precursor fatty acids by platelets. J Clin Invest 1983;72:214-220.
624 25. Fan Y, Støving RK, Berreira Ibraim S et al. The gut microbiota contributes to the pathogenesis
625 of anorexia nervosa in humans and mice. Nat Microbiol 2023;8:787-802.
626 26. Kindschuh WF, Baldini F, Liu MC et al. Preterm birth is associated with xenobiotics and
627 predicted by the vaginal metabolome. Nat Microbiol 2023;8:246-259.
628 27. Vieira-Silva S, Falony G, Belda E et al. Statin therapy is associated with lower prevalence of gut
629 microbiota dysbiosis. Nature 2020;581:310-315.
630 28. Zhao L, Huang Y, Lu L et al. Saturated long-chain fatty acid-producing bacteria contribute to
631 enhanced colonic motility in rats. Microbiome 2018;6:107.
632 29. Li J, Li Y, Ivey KL et al. Interplay between diet and gut microbiome, and circulating
633 concentrations of trimethylamine N-oxide: findings from a longitudinal cohort of US men. Gut
634 2022;71:724-733.
635 30. Zhu W, Gregory JC, Org E et al. Gut Microbial Metabolite TMAO Enhances Platelet
636 Hyperreactivity and Thrombosis Risk. Cell 2016;165:111-124.
637 31. Tang WH, Wang Z, Levison BS et al. Intestinal microbial metabolism of phosphatidylcholine
638 and cardiovascular risk. The New England journal of medicine 2013;368:1575-84.
639 32. Adili R, Hawley M, Holinstat M. Regulation of platelet function and thrombosis by omega-3
640 and omega-6 polyunsaturated fatty acids. Prostaglandins Other Lipid Mediat 2018;139:10-18.
641 33. Schmitz G, Ecker J. The opposing effects of n-3 and n-6 fatty acids. Progress in lipid research
642 2008;47:147-55.
643 34. Harris WS, Mozaffarian D, Rimm E et al. Omega-6 fatty acids and risk for cardiovascular
644 disease: a science advisory from the American Heart Association Nutrition Subcommittee of
645 the Council on Nutrition, Physical Activity, and Metabolism; Council on Cardiovascular
646 Nursing; and Council on Epidemiology and Prevention. Circulation 2009;119:902-7.
647 35. Marklund M, Wu JHY, Imamura F et al. Biomarkers of Dietary Omega-6 Fatty Acids and
648 Incident Cardiovascular Disease and Mortality. Circulation 2019;139:2422-2436.
649 36. Yeung J, Tourdot BE, Adili R et al. 12(S)-HETrE, a 12-Lipoxygenase Oxylipin of Dihomo-gamma-
650 Linolenic Acid, Inhibits Thrombosis via Galphas Signaling in Platelets. Arteriosclerosis,
651 thrombosis, and vascular biology 2016;36:2068-77.
652 37. Nemet I, Saha PP, Gupta N et al. A Cardiovascular Disease-Linked Gut Microbial Metabolite
653 Acts via Adrenergic Receptors. Cell 2020;180:862-877 e22.

654

655 ## Figure legends

656 **Figure 1| Long-chain free fatty acids (LCFAs) dominate the metabolome alterations**
657 **in plasma of early acute myocardial infarction (eAMI) patients compared with**
658 **healthy control (HC) individuals. (a)** Principal component (PC) analysis demonstrates
659 the remarkable metabolome alterations in eAMI patients compared with HC
660 individuals. **(b)** KEGG metabolic pathway enrichment of differential metabolites (FDR-
661 adjusted $p < 0.05$) between eAMI and healthy controls. Fisher's exact test (one-side)
662 followed by FDR-adjusted p value was used and only pathways with FDR-adjusted $p <$
663 0.05 were shown. **(c)** Proportional structure of 32 detected LCFAs in plasma across all
664 samples of eAMI and HC individuals. LCFAs are colored by degree of saturation,
665 saturated LCFAs are colored in yellow, monounsaturated LCFAs are colored in red,
666 and polyunsaturated LCFAs are colored in blue. **(d)** Principal coordinate analysis
667 (PCoA) plot of the difference between eAMI and HC groups based on LCFAs
668 proportion profile. **(e)** Volcano plot of 952 detected metabolites by untargeted
669 metabolome profiling in eAMI patients and HC individuals. Red dots represent
670 significantly up-regulated (FDR-adjusted $p < 0.05$ and Cliff Delta > 0.4) metabolites in
671 eAMI plasma. Blue dots represent notably eAMI-depleted plasma metabolites (FDR-
672 adjusted $p < 0.05$ and Cliff Delta < 0.4). Grey dots marked the unchanged
673 metabolites. Significantly altered LCFAs were labeled. The horizontal line represents
674 FDR cutoff of 0.05 and the vertical lines denote |Cliff Delta| > 0.4.

675 **Figure 2 | Machine learning demonstrates long-chain free fatty acids (LCFAs) are**
676 **potential diagnostic biomarkers for eAMI. (a)** The top 20 most important LCFAs
677 reducing the variance (mean squared error (%IncMSE)) in classification of eAMI by
678 random forest model. %IncMSE denotes the increase in mean squared error of
679 predictions as a result of variable (LCFAs) being permuted. The training model was
680 constructed by proportional profile of 32 LCFAs in 39 training samples. **(b)**
681 Distribution of cross-validation error in random forest classification of eAMI patients
682 as the number of top ranking LCFAs increased. Red dot line marks the optimal
683 number of LCFAs (n = 14) for the classification of eAMI patients. **(c and d)** Receiver
684 operating characteristic (ROC) curve using the 14 LCFAs optimized by random forest

685 model for the (**c**) training and (**d**) test set (right panel, *n* = 17). Vertical heatmap in
686 each panel denotes specificity for the ROC curve in c and d. AUC, area under the
687 curve.

688 **Figure 3 | Bacterial alterations characterize eAMI gut microbiome and greatly**
689 **explain the variance in plasma long-chain free fatty acids (LCFAs)**. **(a)** Density plot
690 showing sample-wide distribution of (% of explained variances) intrinsic factors
691 (gender, age, and body mass index (BMI)) associated with the plasma concentrations
692 of LCFAs. **(b)** Bar plot demonstrates the variation of 32 LCFAs explained by identified
693 bacterial taxa at species level using LASSO regression. **(c)** Stacked bar plot shows the
694 prevalence of gut enterotypes in eAMI and control groups. **(d)** Circular heatmap
695 represents the correlation between LCFAs and gut bacterial species. Only association
696 groups with FDR-adjusted p value of < 0.01 are colored in this plot.

697 **Figure 4 | Alterations in viral gut microbiota between eAMI and HC groups.** Box
698 plots showing the relative abundance of increased **(a)** and decreased **(b)** viral gut
699 microbiota at species level in eAMI gut microbiome compared to that of HC group.
700 Differences in abundance were detected using MaAslin2. **(c)** Significant variations in
701 the abundance, abundance ratios, and counts of virulent and temperate phages
702 between the HC and eAMI groups. Significance was determined by Wilcoxon ranked
703 sum test. For box plots in all panels, the vertical lines extend 1.5 times the
704 interquartile range (top and bottom borders of the box) and the median depicted by
705 the horizontal line inside the box.

706 **Figure 5 | Bacterial structural variations (SVs) links to long-chain free fatty acids**
707 **profiles in acute myocardial infarction (AMI) patients. (a)** Number of SVs of each
708 bacterial species in 56 study participants. **(b)** Pie chart showing the total identified
709 SVs numbers. **(c)** Boxplot of Canberra distance between samples within eAMI and
710 healthy control (HC) groups based on SVs profile, significance is determined by two-
711 sided Mann-Whitney *U*-test. **(d)** Chord diagram showing significant associations
712 between LCFAs and bacterial SVs. **(e)** Heatmap demonstrates the associations
713 between SVs of *Alistipes shahii* and LCFAs. Only significant correlations with FDR-
714 adjusted p value of < 0.01 are visualized. ++, FDR-adjusted p < 0.01, and +++, FDR-

715 adjusted p < 0.001. **(f)** The deletion rate of the 3-kbp deletion harboring 3-oxoacyl-
716 [acyl-carrier protein] reductase (FabG) in *Alistipes shahii*. **(g)** Stacking bar plot
717 represents the prevalence of 3-kbp deletion SV of *Alistipes shahii* in eAMI and HC
718 groups. **(h)** Relative abundance of LCFAs in individuals with and without the 3-kbp
719 deletion SV of *Alistipes shahii*. **, p < 0.01, ***, p < 0.001 determined by two-sided
720 Mann-Whitney *U*-test.

721 **Figure 6 | Early acute myocardial infarction (eAMI)-associated long-chain free fatty**
722 **acids (LCFAs) bind to thrombosis-related receptors and induce thrombosis in**
723 **human platelets. (a)** Heatmap of binding energies between eAMI-associated LCFAs
724 and thrombosis-related receptors through molecular docking. Bing affinities are
725 quantified at kJ/mol. **(b)** The representative AutoDock predicted binding
726 conformation complex of LCFAs versus thrombosis-related receptors, within which
727 the receptors are depicted as cartoons and LCFAs as sticks. **(c)** The thrombogenic
728 impact of eAMI-associated LCFAs on human platelets is depicted in a heatmap.
729 Platelet aggregation ratios of > 10% and 10% are indicated by blue and grey,
730 respectively. **(d)** Representative platelet aggregation curves in a time interval of 300
731 seconds after the treatment of LCFAs at a concentration of 5 mM. Red dashed line
732 indicates 10% threshold.

733

734 ## Supplementary Figures

735 **Figure S1 | Participant flow diagram.** 123 suspected myocardial infarction patients
736 were contacted, and 30 were eventually enrolled after screening.

737 **Figure S2 | a**, Distribution of measured metabolite super pathways of the 952
738 metabolites. **b**, Distribution of metabolite prevalence among the 56 samples. Blue
739 distribution represents prevalence of all analyzed metabolites (*n* = 952). Numbers of
740 metabolites that are present in more than 50% (*n* = 28) of the samples are indicated
741 by dashed lines.

742 **Figure S3 | Metabolic alterations in the plasma of eAMI patients.** Heatmap of

743 contrasted metabolites in the plasma of healthy controls (HC) and eAMI patients.

744 **Figure S4 | Alterations in bacterial gut microbiota in eAMI patients. a**, Phylogenetic
745 tree of contrasted bacterial taxa between eAMI and HC bacterial gut microbiota. Taxa
746 colored in red and blue respectively represents increased and reduced taxa in eAMI
747 bacterial gut microbiota compared with HC group. **b**. Box plot (line, median; box,
748 interquartile range (IQR); whiskers, 1.5× IQR) of β-diversity at bacterial species level
749 (Canberra distance) of eAMI (n = 30) and HC (n = 26) gut microbiota. Statistical
750 significances between two groups were determined by Wilcoxon rank-sum test (two-
751 sided).

752 **Figure S5 | Gut microbiome at genus level associate with long-chain fatty acids**
753 **(LCFAs) metabolism.** Circular heatmap represents the correlation between LCFAs and
754 gut bacteria at genus level. Association groups with FDR-adjusted p value of < 0.05
755 are visualized in this plot.

756 **Figure S6 | Thrombogenic effects of FFA 20:4 (arachidonic acid) in human platelets.**
757 Platelet aggregation curves in a time interval of 300 seconds after the treatment of
758 FFA 20:4 at concentrations of 500 μM and 1 mM are given in **(a)** and **(b)**, respectively.
759 Red dashed line indicates 10% threshold.

760

761 **Table 1. Cohort characteristics**

	eAMI, n = 30[1]	**Control**, n = 26[1]	**p-value**[2]
Sub-classification			
Control	0 (0%)	26 (100%)	
NSTEMI	5 (17%)	0 (0%)	
STEMI	25 (83%)	0 (0%)	
Gender			0.051
Female	3 (10%)	8 (31%)	
Male	27 (90%)	18 (69%)	
Age (ys)	56 (46, 66)	59 (43, 67)	>0.9
BMI（Kg/㎡）	26.4 (22.9, 28.3)	24.4 (22.0, 26.3)	0.2
Smoking (n)	19 (63%)	4 (15%)	<0.001
Alcohol (n)	10 (33%)	2 (7.7%)	0.020
Hypertention (n)	22 (73%)	9 (35%)	0.004
Diabetes (n)	7 (23%)	4 (15%)	0.5
Other commorbidities (n)	4 (13%)	4 (15%)	>0.9
Antithrombiotic (n)	1 (3.3%)	3 (12%)	0.3
Statin (n)	1 (3.3%)	2 (7.7%)	0.6
Antiarrhythmic (n)	2 (6.7%)	2 (7.7%)	>0.9
Antidiabetic (n)	4 (13%)	2 (7.7%)	0.7
Antihypertensive (n)	12 (40%)	8 (31%)	0.5
PPI (n)	1 (3.3%)	1 (3.8%)	>0.9
Culprit vessel (n)			
LM	1 (3.3%)	0 (0%)	>0.9
RCA	16 (53%)	0 (0%)	<0.001
LAD	22 (73%)	0 (0%)	<0.001
LCX	15 (50%)	0 (0%)	<0.001
Emergency troponin (ng/mL)	0 (0, 4)	0 (0, 0)	0.5
Emergency BNP (ng/L)	0.97 (0.13, 2.05)	0.98 (0.98, 0.98)	>0.9
In-hospital troponin (ng/mL)	37 (11, 99)	0 (0, 0)	<0.001
In-hospital Pro-BNP (ng/L)	395 (206, 1,039)	49 (17, 115)	<0.001
LDH (U/L)	0 (0, 473)	133 (133, 133)	0.7
Creatine kinase (U/L)	82 (40, 151)	2 (1, 3)	<0.001
CRP (mg/L)	0.9 (0.0, 3.6)	0.0 (0.0, 0.4)	0.003
WBC (*10^9/L)	12.4 (10.0, 13.3)	5.9 (4.9, 6.6)	<0.001
Neutrophils (%)	79 (73, 86)	57 (49, 65)	<0.001
Lymphocyte (%)	14 (9, 17)	33 (23, 39)	<0.001
Hemoglobin (g/L)	145 (135, 155)	138 (129, 156)	0.5
RDW (%)	12.50 (12.20, 12.78)	12.50 (12.20, 12.95)	0.7
ALT (U/L)	50 (36, 63)	17 (13, 28)	<0.001
AST (U/L)	252 (90, 358)	22 (18, 24)	<0.001
GST/GLT	3.82 (2.66, 5.49)	1.18 (0.88, 1.38)	<0.001
Creatinine (μmol/L)	73 (66, 88)	68 (55, 80)	0.068
BUN/creatinine	0.075 (0.053, 0.080)	0.070 (0.053, 0.090)	0.7
Uric acid (μmol/L)	361 (301, 513)	325 (252, 384)	0.035
Fasting glucose (mmol/L)	5.9 (5.3, 7.9)	4.9 (4.4, 5.2)	<0.001
HbA1C (%)	5.85 (5.53, 6.35)	5.40 (0.00, 5.77)	0.003
GSP (mmol/L)	1.89 (1.72, 2.19)	1.71 (0.35, 1.86)	0.009
Total cholesterol (mmol/L)	5.32 (4.44, 5.93)	4.24 (3.33, 5.18)	0.002
Triglycerides (mmol/L)	1.44 (0.95, 2.79)	1.19 (0.76, 1.53)	0.042
HDL (mmol/L)	1.01 (0.90, 1.10)	1.00 (0.86, 1.24)	0.9

	eAMI, n = 30[1]	**Control**, n = 26[1]	**p-value**[2]
LDL (mmol/L)	3.58 (2.92, 4.18)	2.81 (1.98, 3.16)	<0.001
apoB (g/L)	0.98 (0.82, 1.22)	0.59 (0.10, 0.79)	<0.001
apoA1 (g/L)	1.02 (0.90, 1.09)	1.02 (0.20, 1.22)	>0.9
LP(a) (mg/L)	14 (9, 25)	7 (0, 24)	0.063
SAA (mg/L)	15 (3, 32)	1 (0, 3)	<0.001
U-occult blood (n)			0.035
no	18 (60%)	20 (77%)	
Yes	12 (40%)	4 (15%)	
U-protein (n)			0.051
no	20 (67%)	21 (81%)	
Yes	10 (33%)	3 (12%)	
U-glucose (n)			0.037
no	23 (77%)	23 (88%)	
Yes	7 (23%)	1 (3.8%)	

[1]n (%); Median (IQR)
[2]Fisher's exact test; Pearson's Chi-squared test; Wilcoxon rank sum test
eAMI, early phase of acute myocardial infarction; NSTEMI, non-ST-elevation myocardial infarction; STEMI, ST-elevation myocardial infarction; BMI, body mass index; PPI, proton pump inhibitor; LM, left main; RCA, right coronary artery; LAD, left anterior descending artery; LCX, left circumflex artery; BNP, brain natriuretic peptide; CRP, C-reactive protein; WBC, white blood cell; RDW, red cell distribution width; ALT, alanine transaminase; AST, aspartate transaminase; GST/GLT, glutathione S-transferase; BUN, blood urea nitrogen; HbA1C, hemoglobin A1c; GSP, glycated serum protein; HDL, high-density lipoprotein cholesterol; LDL, low-density lipoprotein cholesterol; apo, apolipoprotein; LP, lipoprotein; SAA, serum amyloid A; U-, uric.

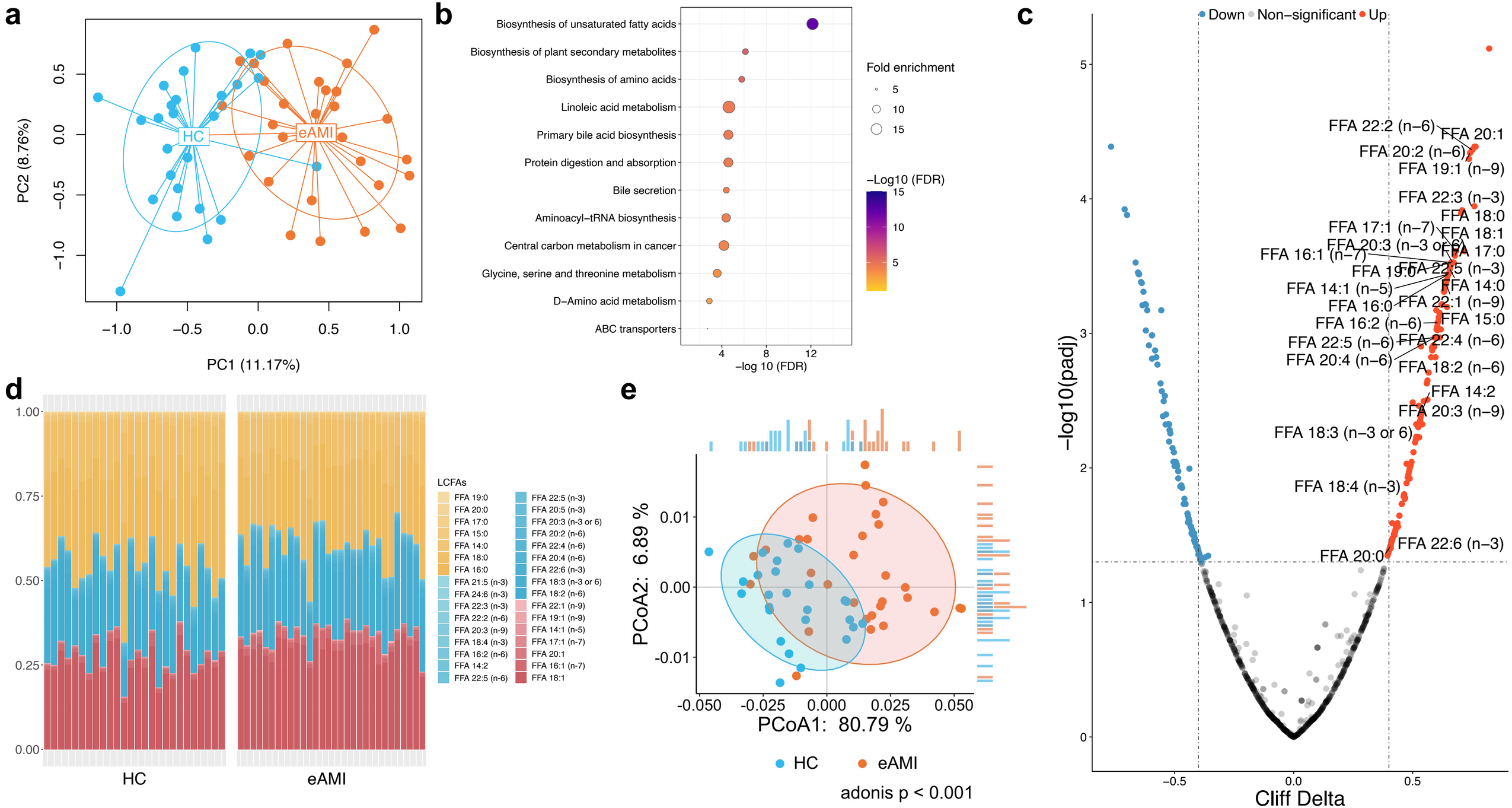
a
HC
eAMI
PC2 (8.76%)
PC1 (11.17%)
b
Biosynthesis of unsaturated fatty acids
Biosynthesis of plant secondary metabolites
Biosynthesis of amino acids
Linoleic acid metabolism
Primary bile acid biosynthesis
Protein digestion and absorption
Bile secretion
Aminoacyl−tRNA biosynthesis
Central carbon metabolism in cancer
Glycine, serine and threonine metabolism
D−Amino acid metabolism
ABC transporters
−log 10 (FDR)
Fold enrichment
−Log10 (FDR)
c
Down
Non−significant
Up
−log10(padj)
Cliff Delta
FFA 22:2 (n−6)
FFA 20:1
FFA 20:2 (n−6)
FFA 19:1 (n−9)
FFA 22:3 (n−3)
FFA 18:0
FFA 17:1 (n−7)
FFA 18:1
FFA 20:3 (n−3 or 6)
FFA 17:0
FFA 16:1 (n−7)
FFA 22:5 (n−3)
FFA 19:0
FFA 14:1 (n−5)
FFA 14:0
FFA 16:0
FFA 22:1 (n−9)
FFA 16:2 (n−6)
FFA 15:0
FFA 22:5 (n−6)
FFA 22:4 (n−6)
FFA 20:4 (n−6)
FFA 18:2 (n−6)
FFA 14:2
FFA 20:3 (n−9)
FFA 18:3 (n−3 or 6)
FFA 18:4 (n−3)
FFA 22:6 (n−3)
FFA 20:0
d
LCFAs
FFA 19:0
FFA 20:0
FFA 17:0
FFA 15:0
FFA 14:0
FFA 18:0
FFA 16:0
FFA 21:5 (n-3)
FFA 24:6 (n-3)
FFA 22:3 (n-3)
FFA 22:2 (n-6)
FFA 20:3 (n-9)
FFA 18:4 (n-3)
FFA 16:2 (n-6)
FFA 14:2
FFA 22:5 (n-6)
FFA 22:5 (n-3)
FFA 20:5 (n-3)
FFA 20:3 (n-3 or 6)
FFA 20:2 (n-6)
FFA 22:4 (n-6)
FFA 20:4 (n-6)
FFA 22:6 (n-3)
FFA 18:3 (n-3 or 6)
FFA 18:2 (n-6)
FFA 22:1 (n-9)
FFA 19:1 (n-9)
FFA 14:1 (n-5)
FFA 17:1 (n-7)
FFA 20:1
FFA 16:1 (n-7)
FFA 18:1
HC
eAMI
e
PCoA2: 6.89 %
PCoA1: 80.79 %
HC
eAMI
adonis p < 0.001

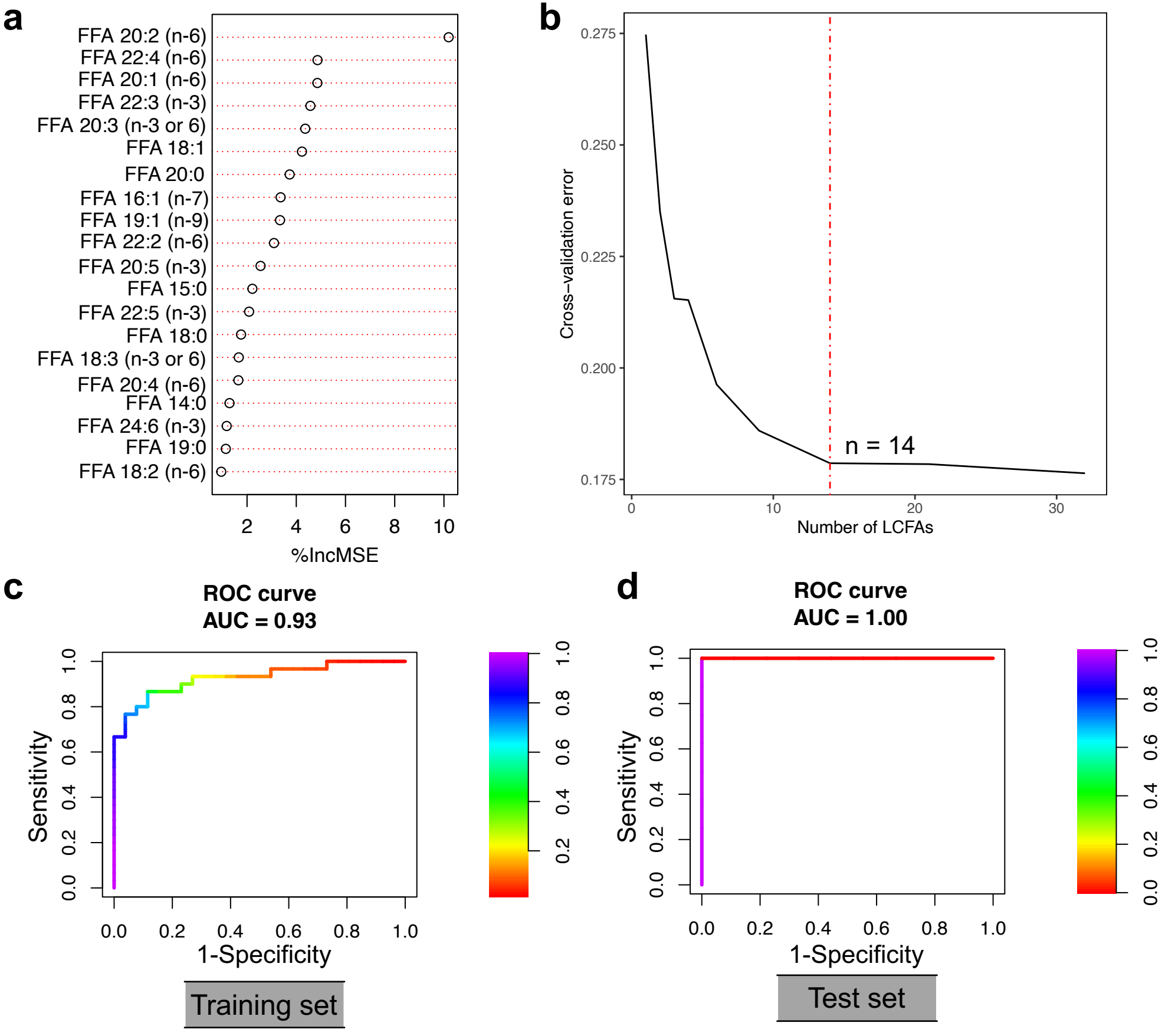
a
FFA 20:2 (n-6)
FFA 22:4 (n-6)
FFA 20:1 (n-6)
FFA 22:3 (n-3)
FFA 20:3 (n-3 or 6)
FFA 18:1
FFA 20:0
FFA 16:1 (n-7)
FFA 19:1 (n-9)
FFA 22:2 (n-6)
FFA 20:5 (n-3)
FFA 15:0
FFA 22:5 (n-3)
FFA 18:0
FFA 18:3 (n-3 or 6)
FFA 20:4 (n-6)
FFA 14:0
FFA 24:6 (n-3)
FFA 19:0
FFA 18:2 (n-6)
2 4 6 8 10
%IncMSE
b
Cross−validation error
0.275
0.250
0.225
0.200
0.175
n = 14
0 10 20 30
Number of LCFAs
c
ROC curve
AUC = 0.93
Sensitivity
0.0 0.2 0.4 0.6 0.8 1.0
1-Specificity
Training set
d
ROC curve
AUC = 1.00
Sensitivity
0.0 0.2 0.4 0.6 0.8 1.0
1-Specificity
Test set

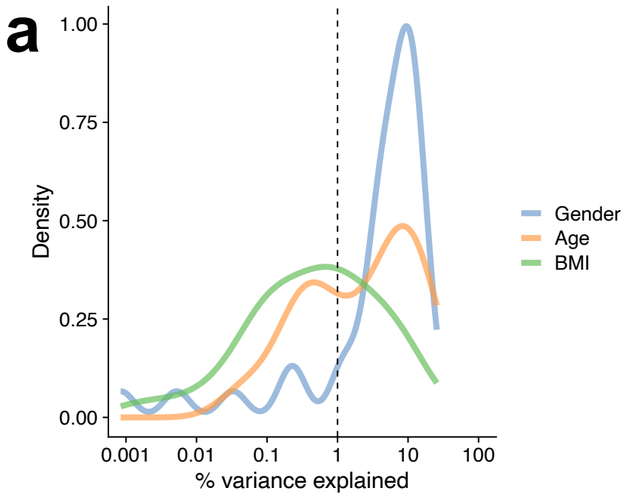
a
Density
1.00
0.75
0.50
0.25
0.00
0.001
0.01
0.1
1
10
100
% variance explained
Gender
Age
BMI

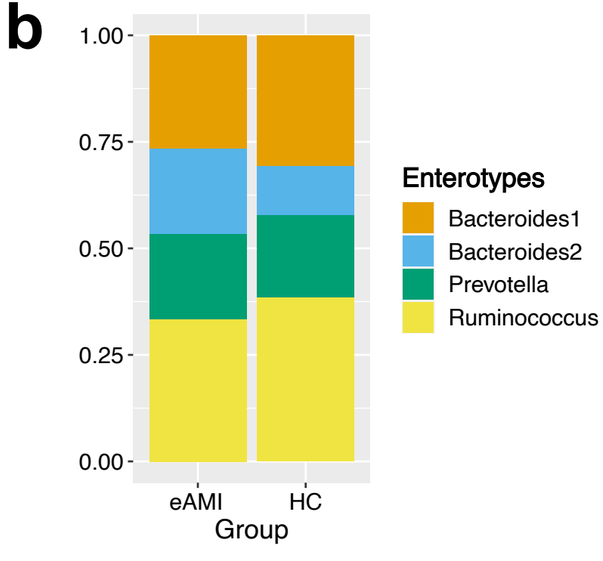
b
1.00
0.75
0.50
0.25
0.00
eAMI
HC
Group
Enterotypes
Bacteroides1
Bacteroides2
Prevotella
Ruminococcus

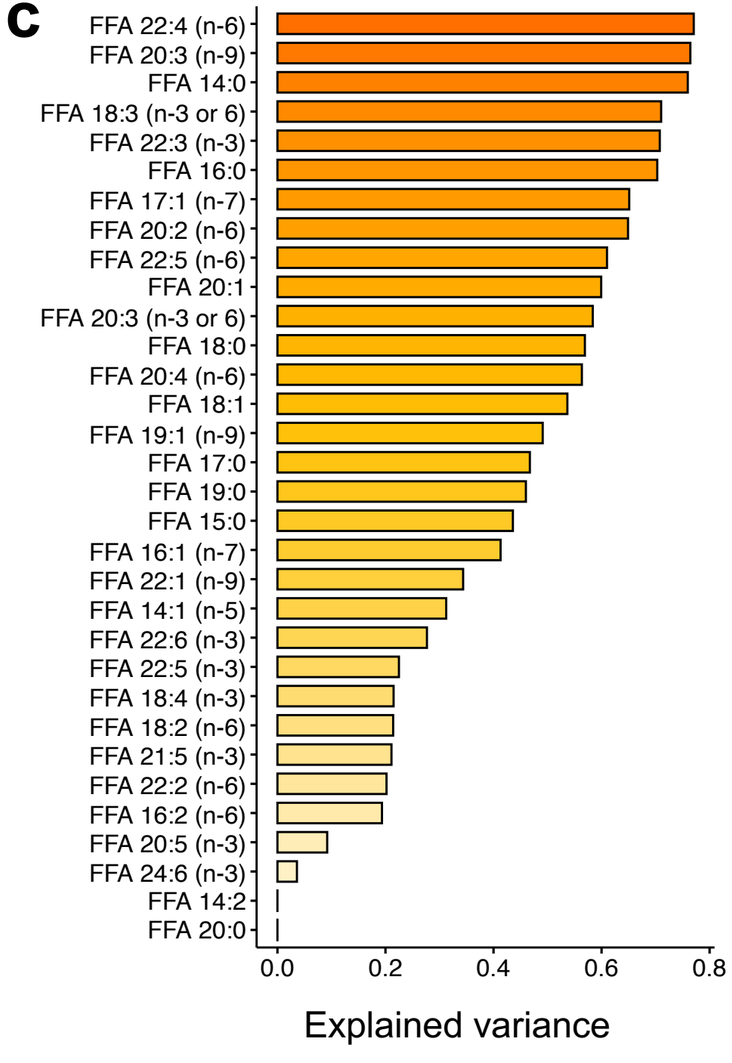
c
FFA 22:4 (n-6)
FFA 20:3 (n-9)
FFA 14:0
FFA 18:3 (n-3 or 6)
FFA 22:3 (n-3)
FFA 16:0
FFA 17:1 (n-7)
FFA 20:2 (n-6)
FFA 22:5 (n-6)
FFA 20:1
FFA 20:3 (n-3 or 6)
FFA 18:0
FFA 20:4 (n-6)
FFA 18:1
FFA 19:1 (n-9)
FFA 17:0
FFA 19:0
FFA 15:0
FFA 16:1 (n-7)
FFA 22:1 (n-9)
FFA 14:1 (n-5)
FFA 22:6 (n-3)
FFA 22:5 (n-3)
FFA 18:4 (n-3)
FFA 18:2 (n-6)
FFA 21:5 (n-3)
FFA 22:2 (n-6)
FFA 16:2 (n-6)
FFA 20:5 (n-3)
FFA 24:6 (n-3)
FFA 14:2
FFA 20:0
0.0
0.2
0.4
0.6
0.8
Explained variance

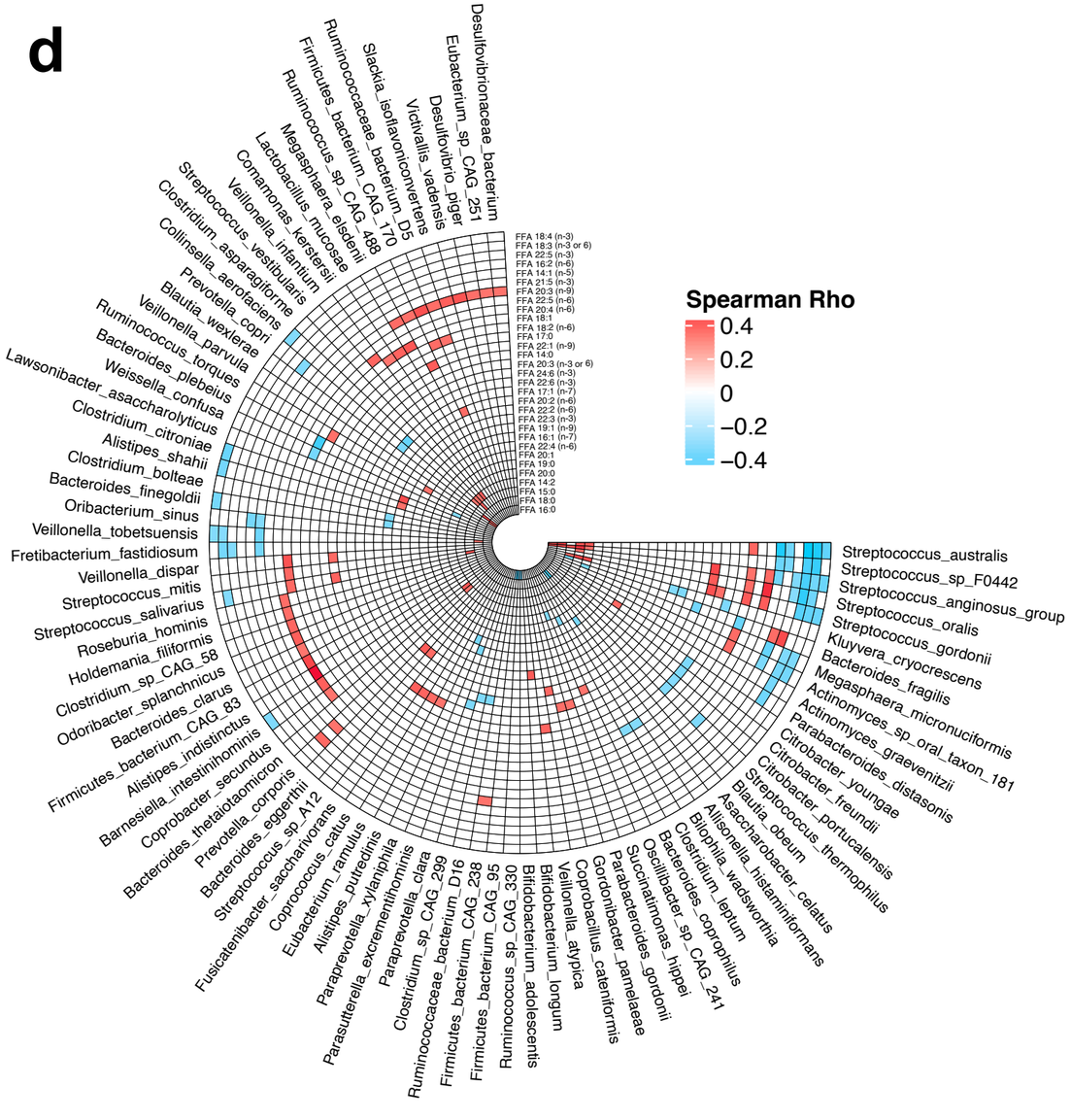
d
Spearman Rho
0.4
0.2
0
−0.2
−0.4
Desulfovibrionaceae_bacterium
Eubacterium_sp_CAG_251
Desulfovibrio_piger
Victivallis_vadensis
Slackia_isoflavoniconverfens
Ruminococcaceae_bacterium_D5
Firmicutes_bacterium_CAG_170
Ruminococcus_sp_CAG_488
Megasphaera_elsdenii
Lactobacillus_mucosae
Coprococcus_kerstersii
Veillonella_intantium
Streptococcus_vestibularis
Clostridium_asparagiforme
Collinsella_aerofaciens
Prevotella_copri
Blautia_wexlerae
Veillonella_parvula
Ruminococcus_torques
Bacteroides_plebeius
Weissella_confusa
Lawsonibacter_asaccharolyticus
Clostridium_citroniae
Alistipes_shahii
Clostridium_bolteae
Bacteroides_finegoldii
Oribacterium_sinus
Veillonella_tobetsuensis
Fretibacterium_fastidiosum
Veillonella_dispar
Streptococcus_mitis
Streptococcus_salivarius
Roseburia_hominis
Holdemania_filiformis
Clostridium_sp_CAG_58
Odoribacter_splanchnicus
Bacteroides_clarus
Firmicutes_bacterium_CAG_83
Alistipes_indistinctus
Barnesiella_intestinihominis
Coprobacter_secundus
Bacteroides_thetaiotaomicron
Prevotella_corporis
Bacteroides_eggerthii
Streptococcus_sp_A12
Fusicatenibacter_saccharivorans
Eubacterium_ramulus
Coprococcus_catus
Alistipes_putredinis
Paraprevotella_xylaniphila
Parasutterella_excrementihominis
Paraprevotella_clara
Clostridium_sp_CAG_299
Ruminococcaceae_bacterium_D16
Firmicutes_bacterium_CAG_238
Firmicutes_bacterium_CAG_95
Ruminococcus_sp_CAG_330
Bifidobacterium_adolescentis
Bifidobacterium_longum
Veillonella_atypica
Coprobacillus_catenformis
Gordonibacter_pamelaeae
Parabacteroides_gordonii
Succinatimonas_hippei
Oscillibacter_sp_CAG_241
Bacteroides_coprophilus
Clostridium_leptum
Bilophila_wadsworthia
Alistipes_histaminiformans
Asaccharobacter_celatus
Blautia_obeum
Streptococcus_thermophilus
Citrobacter_portucalensis
Citrobacter_freundii
Citrobacter_youngae
Parabacteroides_distasonis
Actinomyces_graevenitzii
Actinomyces_sp_oral_taxon_181
Megasphaera_micronuciformis
Bacteroides_fragilis
Kluyvera_cryocrescens
Streptococcus_gordonii
Streptococcus_oralis
Streptococcus_anginosus_group
Streptococcus_sp_F0442
Streptococcus_australis

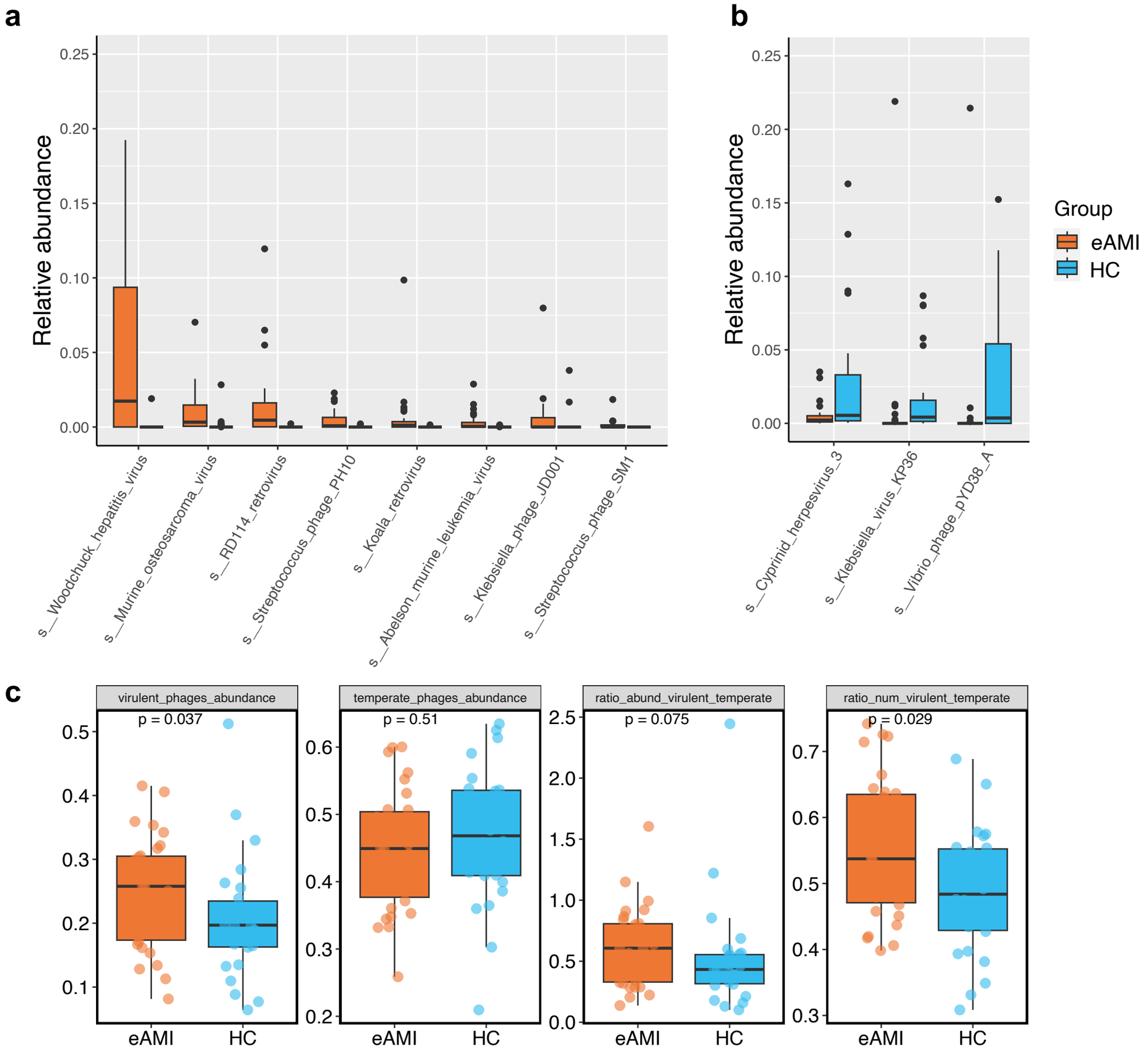
a
Relative abundance
0.25
0.20
0.15
0.10
0.05
0.00
s__Woodchuck_hepatitis_virus
s__Murine_osteosarcoma_virus
s__RD114_retrovirus
s__Streptococcus_phage_PH10
s__Koala_retrovirus
s__Abelson_murine_leukemia_virus
s__Klebsiella_phage_JD001
s__Streptococcus_phage_SM1
b
Relative abundance
s__Cyprinid_herpesvirus_3
s__Klebsiella_virus_KP36
s__Vibrio_phage_pYD38_A
Group
eAMI
HC
c
virulent_phages_abundance
p = 0.037
temperate_phages_abundance
p = 0.51
ratio_abund_virulent_temperate
p = 0.075
ratio_num_virulent_temperate
p = 0.029
eAMI
HC

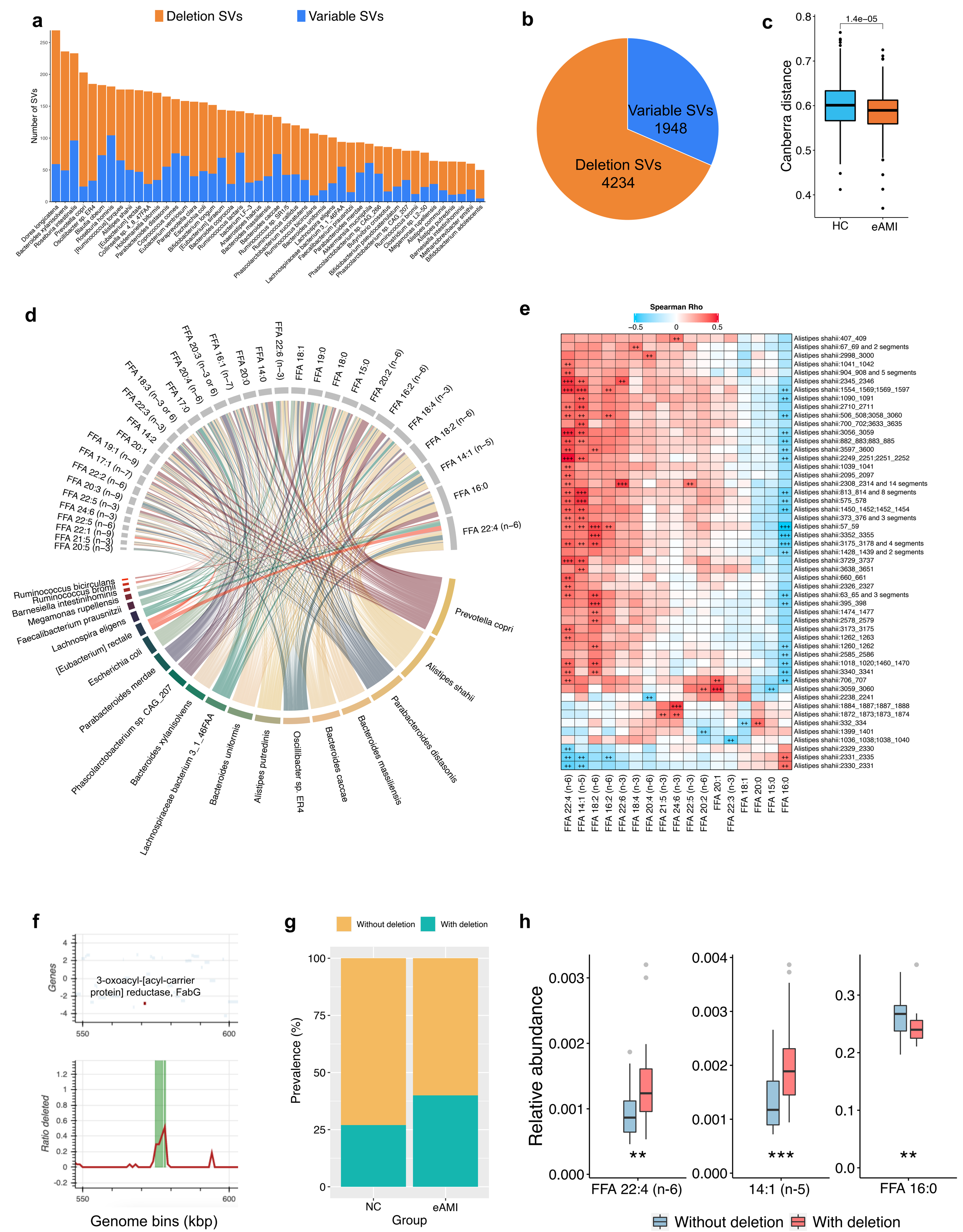
a
Deletion SVs
Variable SVs
Number of SVs
b
Variable SVs
1948
Deletion SVs
4234
c
1.4e−05
Canberra distance
HC
eAMI
d
e
Spearman Rho
−0.5
0
0.5
f
Genes
3-oxoacyl-[acyl-carrier protein] reductase, FabG
Ratio deleted
Genome bins (kbp)
g
Without deletion
With deletion
Prevalence (%)
NC
eAMI
Group
h
Relative abundance
FFA 22:4 (n-6)
14:1 (n-5)
FFA 16:0
Without deletion
With deletion

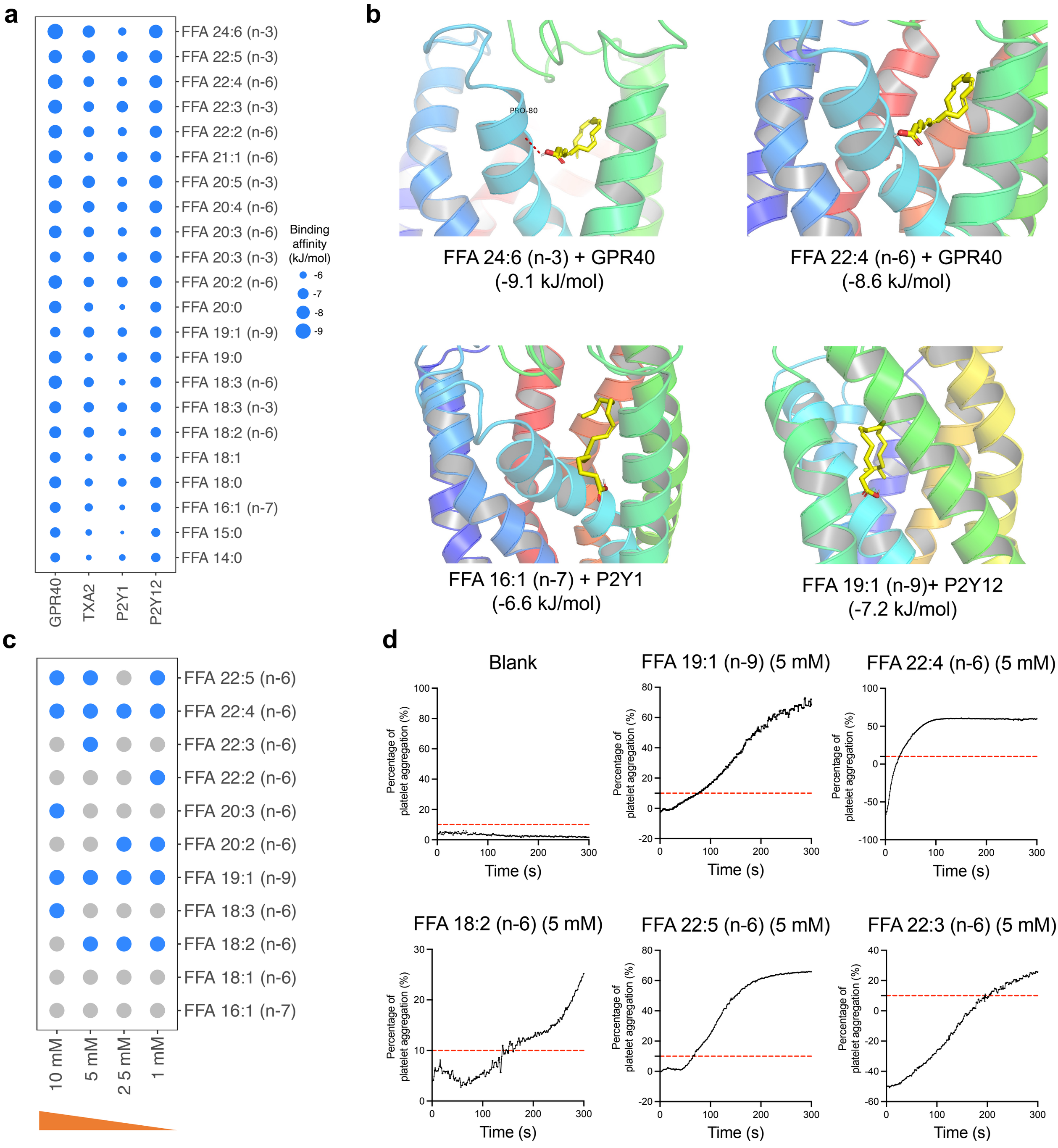
a
FFA 24:6 (n-3)
FFA 22:5 (n-3)
FFA 22:4 (n-6)
FFA 22:3 (n-3)
FFA 22:2 (n-6)
FFA 21:1 (n-6)
FFA 20:5 (n-3)
FFA 20:4 (n-6)
FFA 20:3 (n-6)
FFA 20:3 (n-3)
FFA 20:2 (n-6)
FFA 20:0
FFA 19:1 (n-9)
FFA 19:0
FFA 18:3 (n-6)
FFA 18:3 (n-3)
FFA 18:2 (n-6)
FFA 18:1
FFA 18:0
FFA 16:1 (n-7)
FFA 15:0
FFA 14:0
GPR40
TXA2
P2Y1
P2Y12
Binding affinity (kJ/mol)
-6
-7
-8
-9
b
PRO-80
FFA 24:6 (n-3) + GPR40
(-9.1 kJ/mol)
FFA 22:4 (n-6) + GPR40
(-8.6 kJ/mol)
FFA 16:1 (n-7) + P2Y1
(-6.6 kJ/mol)
FFA 19:1 (n-9)+ P2Y12
(-7.2 kJ/mol)
c
FFA 22:5 (n-6)
FFA 22:4 (n-6)
FFA 22:3 (n-6)
FFA 22:2 (n-6)
FFA 20:3 (n-6)
FFA 20:2 (n-6)
FFA 19:1 (n-9)
FFA 18:3 (n-6)
FFA 18:2 (n-6)
FFA 18:1 (n-6)
FFA 16:1 (n-7)
10 mM
5 mM
2.5 mM
1 mM
d
Blank
FFA 19:1 (n-9) (5 mM)
FFA 22:4 (n-6) (5 mM)
FFA 18:2 (n-6) (5 mM)
FFA 22:5 (n-6) (5 mM)
FFA 22:3 (n-6) (5 mM)
Percentage of platelet aggregation (%)
Time (s)